Theory of Ultrafast Dynamics of Electron-Phonon Interactions in Two Dimensional Electron Gases: Semiconductor Quantum Wells, Surfaces and Graphene

Marten Richter[1], Stefan Butscher[1], Norbert Bücking[1], Frank Milde[1], Carsten Weber[2], Peter Kratzer[3], Matthias Scheffler[4], and Andreas Knorr[1]

[1] Institut für Theoretische Physik, Technische Universität Berlin, Hardenbergstr. 36, 10623 Berlin, Germany
marten.richter@tu-berlin.de
[2] Mathematical Physics, Lund University, Box 118, 22100 Lund, Sweden
[3] Fachbereich Physik, Universität Duisburg-Essen, Lotharstr. 1, 47048 Duisburg, Germany
[4] Fritz-Haber-Institut der Max-Planck-Gesellschaft, Faradayweg 4-6, 14195 Berlin, Germany

Abstract. Two-dimensional semiconductors are ideal model systems for investigating the dynamics of the electron-phonon interaction under spatial confinement of electronic excitations. In this contribution, the simultaneous quantum dynamics of electrons and phonons on ultrafast timescales is theoretically addressed. Typical examples include the ultrafast electron transfer at silicon surfaces, optical intersubband transitions in doped quantum wells, and non-equilibrium phonon generation in graphene.

1 Introduction

Two-dimensional electron gases appear in different semiconductor and semimetal nano-structures like quantum wells [1, 2, 3], graphene [4, 5, 6], and at surfaces [7, 8]. Recent experiments focus on the ultrafast dynamics of these 2D electron gases. A theoretical description of relaxation processes in such systems at low electronic densities and high temperature requires an understanding of how electrons interact with the vibrations of the lattice (phonons)[9, 10].

The main goal of this paper is to give a brief introduction to the theory of optical response for different electron gases and an overview of corresponding experimental investigations. The paper is organized as follows: First, the Hamilton operator is introduced and calculation techniques are presented. Second, the phonon-induced relaxation dynamics of electronic excitations at

the Silicon (001) 2x1 surface is described. Third and fourth, electron-phonon scattering processes in quantum cascade lasers and non-equilibrium phonons in graphene are described. Finally, the scattering-induced quantum emission of an equilibrium 2D electron gas is addressed.

2 Theoretical framework

2.1 Hamilton operator

In order to investigate the dynamics of a 2D electron gas, including many-particle effects, the Hamilton operator of the system has to be specified. Here, we focus on the interaction of electrons with phonons. The Hamilton operator for the free phonons and electron dynamics reads:

$$H_0 = \sum_{l\boldsymbol{k}} \varepsilon_{l\boldsymbol{k}} a^\dagger_{l\boldsymbol{k}} a_{\boldsymbol{k}} + \sum_{\boldsymbol{q}} \hbar\omega_{LO} b^\dagger_{\boldsymbol{q}} b_{\boldsymbol{q}}. \tag{1}$$

The operators $a^\dagger_{l\boldsymbol{k}}$, $a_{l\boldsymbol{k}}$ and $b^\dagger_{\boldsymbol{q}}$, $b_{\boldsymbol{q}}$ are the creation and annihilation operators for electrons and phonons. In most examples below, optical phonons with a phonon frequency ω_{LO} and quasi momentum $\boldsymbol{q}$ are considered, apart from Section 3, where acoustic phonons have been included as well. For the electronic states, the 2D momentum $\boldsymbol{k}$ and a (sub-) band index l are introduced as quantum numbers. The electron phonon interaction reads [10, 11]:

$$H_{\mathrm{EPI}} = \sum_{n\boldsymbol{k},n'\boldsymbol{k}',\boldsymbol{q}} g^{n'\boldsymbol{k}'}_{n\boldsymbol{k},\boldsymbol{q}} a^\dagger_{n\boldsymbol{k}} a_{n'\boldsymbol{k}'} b_{i\boldsymbol{q}} + h.a. \quad . \tag{2}$$

Here, g is the electron-phonon coupling element describing on the phonon-induced electronic transitions. To describe optical excitation, the interaction with the electrical field is included as well. As long as spontaneous emission can be neglected, a classical description of the electrical field through the vector potential $\boldsymbol{A}(t)$ within the dipole approximation is chosen [12]:

$$H_{\mathrm{ext-field}} = \sum_{\boldsymbol{k}n\neq n'} \mathbf{A}(t)\mathbf{p}^{n'\boldsymbol{k}}_{n\boldsymbol{k}}\, a^\dagger_{n\boldsymbol{k}} a_{n'\boldsymbol{k}}. \tag{3}$$

If spontaneous emission is considered, the interaction with the electromagnetic field has to be formulated using photon operators $c^\dagger, c$ [13]:

$$H_{qfield} = \sum_{\boldsymbol{k}\boldsymbol{k}'n\neq n'} \left(\mathbf{F}^{n'\boldsymbol{k}'}_{n\boldsymbol{k}Ks} c^\dagger_{Ks} + (\mathbf{F}^{n\boldsymbol{k}}_{n'\boldsymbol{k}'Ks})^* c_{Ks}\right) a^\dagger_{n\boldsymbol{k}} a_{n'\boldsymbol{k}}, \tag{4}$$

$$H_{0,phtn} = \hbar \sum_{Ks} \omega_{Ks} c^\dagger_{Ks} c_{Ks}. \tag{5}$$

Here, photon modes are characterized by their momentum indices K, polarization s and their frequency ω_{Ks}.

2.2 Dynamics

The electron dynamics of macroscopic quantities, such as the real space density, can be described via the electronic transitions $p^{m\mathbf{l}}_{n\boldsymbol{k}} := \langle a^\dagger_{n\boldsymbol{k}} a_{m\mathbf{l}}\rangle$, electronic (sub-)band densities $f_{n\boldsymbol{k}} := \langle a^\dagger_{n\boldsymbol{k}} a_{n\boldsymbol{k}}\rangle$, where $\langle \ldots \rangle$ denotes the quantum mechanical expectation value of the operator combination. The equations for these quantities are derived using the Heisenberg equation. As a typical example the equation for the polarization is presented [11]:

$$\begin{aligned} i\hbar \frac{d}{dt} p^{m'\mathbf{l}'}_{m\mathbf{l}} = \big(\varepsilon_{m\mathbf{l}} - \varepsilon_{m'\mathbf{l}'}\big) p^{m'\mathbf{l}'}_{m\mathbf{l}} + \mathbf{A}(t) \sum_{n\mathbf{k}} \Big(\mathbf{p}^{n\mathbf{k}}_{m\mathbf{l}} p^{m'\mathbf{l}'}_{n\mathbf{k}} - \mathbf{p}^{m'\mathbf{l}'}_{n\mathbf{k}} p^{n\mathbf{k}}_{m\mathbf{l}} \Big) \\ + \sum_{n\mathbf{k},i\mathbf{q}} \Big(g^{n\mathbf{k}}_{m\mathbf{l},i\mathbf{q}} \Big(s^{n\mathbf{k}}_{m'\mathbf{l}',i\mathbf{q}}\Big)^* + g^{n\mathbf{k}}_{m\mathbf{l},i\mathbf{q}} s^{m'\mathbf{l}'}_{a_{n\mathbf{k}},i\mathbf{q}} - g^{m'\mathbf{l}'}_{n\mathbf{k},i\mathbf{q}} \Big(s^{m\mathbf{l}}_{n\mathbf{k},i\mathbf{q}}\Big)^* \\ - g^{m'\mathbf{l}'}_{n\mathbf{k},i\mathbf{q}} s^{n\mathbf{k}}_{m\mathbf{l},i\mathbf{q}} \Big), \end{aligned} \tag{6}$$

where phonon assisted quantities $s^{m'\mathbf{l}'}_{m\mathbf{l},i\mathbf{q}} = \langle a^\dagger_{m\mathbf{l}} a_{m'\mathbf{l}'} b_{i\mathbf{q}}\rangle$ appear. It is obvious that Eq. (6) is not directly solvable, since it couples to phonon-assisted densities, whose dynamics have to be derived as well:

$$\begin{aligned} i\hbar \frac{d}{dt} \big(s^{m\mathbf{l}}_{m'\mathbf{l}'i\boldsymbol{q}}\big)^* = \big(\varepsilon_{m\mathbf{l}} - \varepsilon_{m'\mathbf{l}'} + \hbar\omega_{i\mathbf{q}}\big) \big(s^{m\mathbf{l}}_{m'\mathbf{l}',i\boldsymbol{q}}\big)^* \\ + \mathbf{A}(t) \sum_{n\mathbf{k}} \Big(\mathbf{p}^{n\mathbf{k}}_{m\mathbf{l}} \big(s^{n\mathbf{k}}_{m'\mathbf{l}',i\boldsymbol{q}}\big)^* - \mathbf{p}^{m'\mathbf{l}'}_{n\mathbf{k}} \big(s^{m\mathbf{l}}_{n\mathbf{k},i\boldsymbol{q}}\big)^* \Big) \\ + \sum_{n\mathbf{k},i'\mathbf{q}'} \Big(g^{n\mathbf{k}}_{m\mathbf{l},i'\mathbf{q}'} \Big(R^{m'\mathbf{l}',i'\boldsymbol{q}'}_{n\boldsymbol{k},i\boldsymbol{q}}\Big)^* + g^{n\mathbf{k}}_{m\mathbf{l},i'\mathbf{q}'} T^{m'\mathbf{l}',i'\boldsymbol{q}'}_{n\boldsymbol{k},i\boldsymbol{q}} \\ - g^{m'\mathbf{l}'}_{n\mathbf{k},i'\mathbf{q}'} \Big(R^{n\mathbf{k},i'\boldsymbol{q}'}_{m\mathbf{l},i\boldsymbol{q}}\Big)^* - g^{m'\mathbf{l}'}_{n\mathbf{k},i'\mathbf{q}'} T^{n\mathbf{k}',i'\boldsymbol{q}'}_{m\mathbf{l},i\boldsymbol{q}} \Big) \\ + \sum_{n\mathbf{k},n'\mathbf{k}'} g^{n'\mathbf{k}'}_{n\mathbf{k},i\mathbf{q}} \langle a^\dagger_{m\mathbf{l}} a^\dagger_{n\mathbf{k}} a_{m'\mathbf{l}'} a_{n'\mathbf{k}'}\rangle. \end{aligned} \tag{7}$$

Within the spirit of a correlation expansion, the terms $R^{m\mathbf{l},i'\boldsymbol{q}'}_{n\boldsymbol{k},i\boldsymbol{q}} = \langle a^\dagger_{n\boldsymbol{k}} a_{m\mathbf{l}} b_{i\boldsymbol{q}} b_{i'\boldsymbol{q}'}\rangle$ and $T^{m\mathbf{l},i'\boldsymbol{q}'}_{n\boldsymbol{k},i\boldsymbol{q}} = \langle a^\dagger_{n\boldsymbol{k}} a_{m\mathbf{l}} b^\dagger{}_{i\boldsymbol{q}} b_{i'\boldsymbol{q}'}\rangle$ are factorized at the second order Born level ($(g^{n'\mathbf{k}'}_{n\mathbf{k},i\mathbf{q}})^2$ or coupled to higher-order correlations within a self-consistent Born approximation [14, 15]. In second-order Born approximation, we obtain e.g: $\langle a^\dagger_{n\boldsymbol{k}} a_{m\mathbf{l}} b^\dagger{}_{i\boldsymbol{q}} b_{i'\boldsymbol{q}'}\rangle \approx \langle a^\dagger_{n\boldsymbol{k}} a_{m\mathbf{l}}\rangle \langle b^\dagger{}_{i\boldsymbol{q}} b_{i'\boldsymbol{q}'}\rangle$. Depending on the situation, occuring phonon occupations $n_{i\boldsymbol{q}} = \langle b^\dagger_{i\boldsymbol{q}} b_{i\boldsymbol{q}}\rangle$ might be treated within a bath approximation or calculated dynamically within the same second-order Markov Born approximation to consider non-equilibrium phonon distributions. Here, as example, the dynamic phonon density equation, later discussed for calculations non equilibriuum calculations in graphene, is given[16]:

$$\dot{n}_{\mathbf{q}} = \frac{2\pi}{\hbar} \sum_{i,\mathbf{k}} |g_{\mathbf{k},\mathbf{q}}|^2 \delta(-\varepsilon_{i\mathbf{k}} + \varepsilon_{i\mathbf{k}+\mathbf{q}} - \hbar\omega_{\mathbf{q}}) \times[(n_{\mathbf{q}}+1) f^+_{i\mathbf{k}+\mathbf{q}} f^-_{i\mathbf{k}} - n_{\mathbf{q}} f^+_{i\mathbf{k}} f^-_{i\mathbf{k}+\mathbf{q}}]. \tag{8}$$

We have introduced $f^+_{i\mathbf{k}} := f_{i\mathbf{k}}$ and $f^-_{i\mathbf{k}} := (1-f_{i\mathbf{k}})$ and kept indices relevant for the graphene case. Within the same level of the Born-Markov approximation, the equations for the electron distributions read [10, 11]:

$$\frac{d}{dt} f_{n\boldsymbol{k}} = 2 \sum_{n'} \left(\Gamma^{n'\,in}_{n\boldsymbol{k}} (1 - f_{n\boldsymbol{k}}) - \Gamma^{n'\,out}_{n\boldsymbol{k}} f_{n\boldsymbol{k}} \right), \tag{9}$$

$$\Gamma^{n'\,in}_{n\boldsymbol{k}} = \frac{\pi}{\hbar} \sum_{\boldsymbol{k}'\boldsymbol{q}\pm} \left| g^{n'\boldsymbol{k}'}_{n\boldsymbol{k},i\boldsymbol{q}} \right|^2 \delta(\epsilon_{n\boldsymbol{k}} - \epsilon_{n'\boldsymbol{k}'} \pm \hbar\omega_{i\boldsymbol{q}}) (n_{\boldsymbol{q}} + \frac{1}{2} \pm \frac{1}{2}) f_{n'\boldsymbol{k}'},$$

$$\Gamma^{n'\,out}_{n\boldsymbol{k}} = \frac{\pi}{\hbar} \sum_{\boldsymbol{k}'\boldsymbol{q}\pm} \left| g^{n'\boldsymbol{k}'}_{n\boldsymbol{k},i\boldsymbol{q}} \right|^2 \delta(\epsilon_{n\boldsymbol{k}} - \epsilon_{n'\boldsymbol{k}'} \pm \hbar\omega_{i\boldsymbol{q}}) (n_{\boldsymbol{q}} + \frac{1}{2} \mp \frac{1}{2}) (1 - f_{n'\boldsymbol{k}'}).$$

Eqs. (8-9) form a selfconsistent set of equations. To describe the system accurately enough in a weak coupling regime, the used approximations might already be sufficient. For stronger coupling regimes, the influence of higher electron-phonon couplings have to be included at least approximatively (cf. [14, 15]).

3 Phonon-induced relaxation dynamics at the Silicon (001) 2×1 surface

Due to the interest in device miniaturisation, electron relaxation effects at semiconductor surfaces play an increasing role in recent research. In contrast to embedded low-dimensional quantum systems (quantum dots, quantum wells), where the band structure and the matrix elements $g^{n'\boldsymbol{k}'}_{n\boldsymbol{k};i\boldsymbol{q}}$ may be described a few parameters (effective masses, dielectric constant, etc. [17]), ab initio calculations are typically necessary to calculate the dynamics of a surface structure [18]: In our approach, density-functional theory (DFT) is used to obtain Kohn-Sham-orbitals to calculate the matrix elements, e.g. Eq. (6),(2). The evaluation of the dynamics is performed in two steps: first, the DFT calculations are processed for a silicon (001) 2×1 surface and all interaction matrix elements $g^{n'\boldsymbol{k}'}_{n\boldsymbol{k};i\boldsymbol{q}}$ and the relevant electronic bandstructure $\varepsilon_{l\boldsymbol{k}}$ are determined from the Kohn-Sham wavefunctions, and, in a second step, are inserted into the dynamical equations (9). Equation (9) describes the electron relaxation dynamics for fixed phonon distributions (bath approximation), after the injection of a non-equilibrium electron occupation via optical excitation [11].

The resulting dynamics of the phonon-induced relaxation of hot electrons within the conduction bands for the silicon (001) 2×1 surface [7, 8] is dominated by two timescales, cf. Fig. 1, which shows the partial relaxation from

surface states to bulk states on short times and then back to surface states after longer times. The two timescales can be rationalized to different relaxation processes due to acoustic and optical phonons and specific features of the bandstructure of the Si (001) surface. In addition to the bulk bands, a surface-related conduction band (D^{down}-band) is partly located in the semiconductor band gap (and thus constitutes the conduction band minimum at the $\overline{\Gamma}$-point).

While the relaxation within the bulk and within the D^{down}-band is fast (1 ps), the interband relaxation from the bulk to the D^{down}-band is much slower [8, 11, 19]. Starting from an optical excitation process with a 1.69 eV pulse of 50 fs duration, the relaxation of optically injected electrons is rather complex: Initially, almost the whole population in the conduction bands is found in the D^{down}-band at an energy about 0.4 eV above the bulk conduction minimum. In Figure 1, this can be seen by a real space population located near the surface after injection at $t = 0$ps (lhs). At a later timestep (2 ps), the conduction band population distributes into the bulk: by phonon emission, a part of the population is transfered from the D^{down}-band to the bulk bands [15]. At the end of the relaxation, we find the entire population near the surface again. The final quasi equilibrium state is the total conduction band minimum (a D^{down}-state at the $\overline{\Gamma}$-point), and all relaxation channels lead to this final energetically lowest state, spatially located at the surface.

By combining the density matrix formalism with density-functional theory and applying it to a silicon 2×1 (001) surface structure, the timescale for the

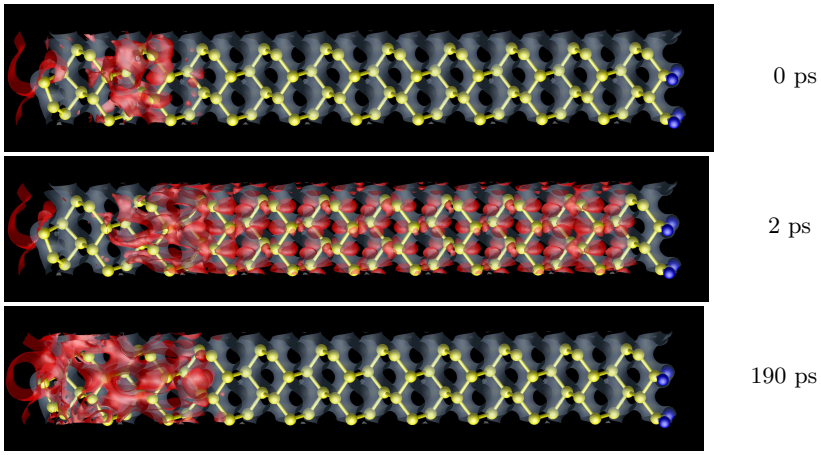

Fig. 1. Projection of the conduction band population into real space for timesteps of 0, 2 and 190 ps. While the initial population is strongly localized at the surface, the population partly shifts to the bulk at 2 ps, and finally returns into a surface state (minimum of D^{down}-band).

fast relaxation process in the D^{down} band of about 1 ps has been obtained in good agreement with experimental findings [7, 8, 19].

4 Scattering response and spatiotemporal wavepackets in Quantum Cascade Lasers

In this section, ultrafast dynamics of the subband population and spatial electronic density evolution in quantum cascade lasers is considered. The quantum cascade laser (QCL) is an electrically pumped intersubband laser consisting of up to several hundreds of quantum wells [20, 21]. Via scattering and tunneling processes, the electrons move from the injector into the active region of one period where the laser transition takes place. The electrons are then collected in the injector of the next period, leading to a cascade of emitted photons. Through engineering of the quantum well widths and potential offsets, the lifetimes and energies of the quantum states can be designed to obtain optimal lasing conditions. For instance, in many THz devices, an inversion is obtained by depleting the lower laser subband on a short time scale via emission of longitudinal optical (LO) phonons [cf. Fig. 2(a)].

In our approach, the interaction of the electronic system with LO phonons and ionized doping centers is described within a second order Born-Markov and bath approximation [cp. Eq. (9)]. The complex multi-period structure is modelled by considering only interaction of next-neighbor elementary cells of the superlattice and applying periodic boundary conditions to the density matrix and the coupling elements [22].

In Fig. 2(b), the dynamics of the subband populations $f_n = 2/A \sum_{\boldsymbol{k}} f_{n\boldsymbol{k}}$ of the THz QCL structure, discussed in Ref. [23], is shown at $T = 10$ K. Here, a strong 170 fs pump pulse saturates the gain inversion at the transistion $3 \rightarrow 2$, leading to Rabi flopping of the involved subbands [22]. After the passage of the pulse, non-radiative relaxation from the lower laser state into subband 1 via phonon emission depletes the population in subband 2,

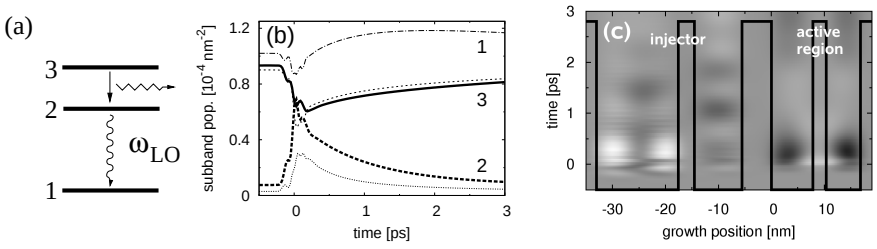

Fig. 2. (a) Resonant phonon design of THz QCL with the laser states 2, 3. The transition $2 \rightarrow 1$ depletes the lower laser level through phonon emission. (b) subband population dynamics for an excitation with a strong ultrafast pulse. (c) Corresponding spatiotemporal evolution of the electronic density (barriers are shown).

while the upper laser state 3 is refilled due to elastic scattering from the injector states of the prior period. The population dynamics is dominated by incoherent evolution after the passage of the pulse i.e. by the cooling of the electron distributions within the spatially extended structure. Fig. 2(c) shows the corresponding spatiotemporally resolved evolution of the electronic density $n(z,t) = 2/A \sum_{n,m} \xi_n^*(z)\, \xi_m(z) \sum_{\boldsymbol{k}} p_{n\boldsymbol{k}}^{m\boldsymbol{k}}(t)$, where $\xi_n(z)$ denotes the envelope of the quantum confined state (white denotes excess, black decreased density compared to the stationary values). Shortly after the pulse, the electronic density in level 3 in the active region is reduced due to the gain saturation of the laser transitions. After this, the system slowly returns to the stationary state on a picosecond time scale. In addition, coherent effects such as density (gain) oscillations between the injector and the active region can be observed. They result from a coherent charge transfer through the main tunneling barrier connecting the two regions [24, 25].

As can be seen, optically induced electron-phonon scattering dynamics in quantum cascade laser reveals the relaxation channels of the structure as well as coherent effects due to resonant tunneling through the barriers[22].

5 Non-equilibrium phonon dynamics in graphene

When peeling off the graphite constituting slices of honeycomb-arranged carbon atoms to the thinnest possible form, mono-layered '2D-graphite' – or graphene – can be produced. Due to its unique electronic properties, graphene has recently drawn a lot of attention: For example, theoretical investigations focused on the quasiparticle properties and dynamics of so-called Dirac-Fermions [26] or electron-phonon interaction [27]. Recently also ultrafast relaxation processes of photo-excited electrons have been studied in experiments [6].

In this section, the relaxation of an optically excited conduction band carrier population into thermal equilibrium by energy dissipation through phonon emission is discussed [16]. It turns out that, for a proper understanding, the dynamics of photo-excited electrons and heated phonons in graphene has to be treated simultaneous. Given optical phonon energies of almost 200 meV and an intermediately strong electron-phonon interaction, the latter process provides an efficient cooling mechanism in this two dimensional system. The relevant quantities for the dynamics are the interband coherence $p_{\boldsymbol{k}}$ at wave vector $\boldsymbol{k}$, the valence (v) and conduction (c) band population $f_{i\boldsymbol{k}}$ ($i = c, v$), as well as the phonon occupation number $n_{\boldsymbol{q}}$ at wave vector $\boldsymbol{q}$, all defined around Eq. (6) in the introduction. We treat the electron-phonon interaction within second-Born Markov equations, known as Bloch-Boltzmann-Peierls equations, Eqs. (8),(9). To determine the electron-phonon coupling (EPC) matrix elements $g_{\boldsymbol{k},\boldsymbol{q}}$ Kohn anomalies in the phonon dispersions are used [27]. The EPC matrix elements describe intravalley (Γ-phonons) as well as intervalley ($\boldsymbol{K}$-

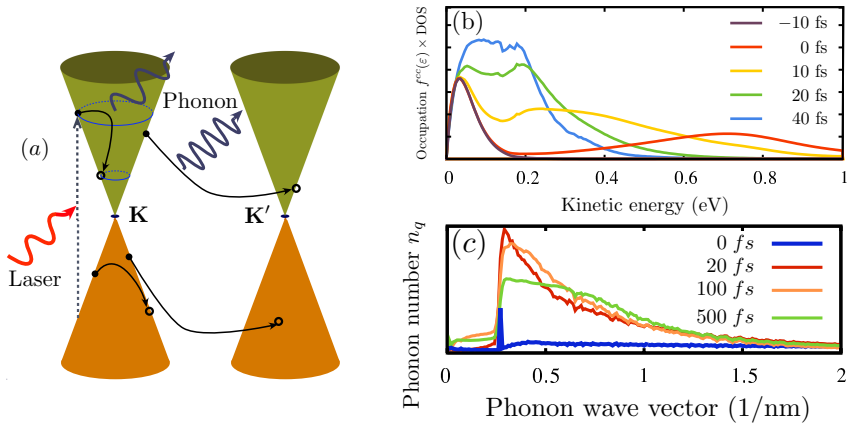

Fig. 3. (a) After laser excitation into the conduction band electrons in the graphene sample relax via intra- and intervalley scattering with optical phonons.(b) shows the temporal evolution of the conduction band occupation f_{ck} times the DOS. Here f_{ck} has been integrated with respect to the angle. (c) shows the occupation of the $\Gamma - E_{2g,LO}$ phonon mode of graphene for different times.

phonons) scattering processes. Due to the anisotropic optical matrix elements [28] anisotropic optical excitation and relaxation processes occur.

Results of the coupled dynamics are shown in Figure 3. Electron relaxation of a photo-excited non-equilibrium distribution takes place on a femtosecond timescale, but is dramatically slowed down after 20 fs. The early drastic electron cooling (b) results in formation of a finite population of the initially quasi unoccupied phonon modes (c). Hot phonons (c) clearly reduce the possibility of energy dissipation by the electronic system after 20 fs.

Our findings provide insight into the ultrafast dynamics of the first 500 fs after excitation not yet accessible by experiment. We show that generation of non-equilibrium (hot) phonons has a noticeable impact on the relaxation dynamics of the excited carriers.

6 Terahertz light emission

In this section we focus on the spontaneous terahertz (THz) quantum emission from a 2D equilibrium electron gas in a doped semiconductor quantum well [13]. Only one subband in effective mass approximation inside the quantum well is considered. The interaction of the electron gas with the light field is treated using a quantized light field Eq. (5) considering a spatially inhomogeneous and frequency dependent dielectric function of the well environment[29, 30, 13, 31]. This allows one to incorporate also the sample geometry and the influence of transversal optical (TO)-phonons of the barrier material, having similar resonance frequency as the electron gas THz

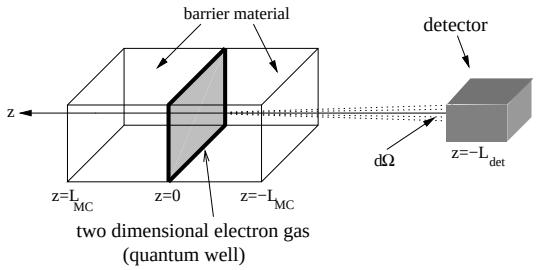

Fig. 4. Geometric setup of the terahertz quantum light emission.

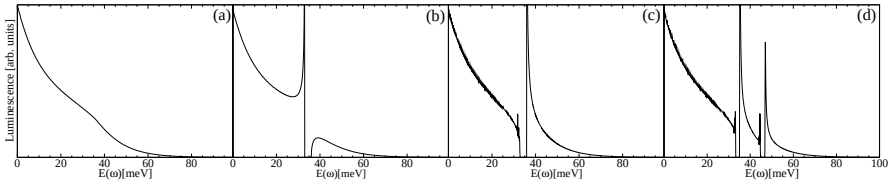

Fig. 5. Luminescence of a Fermi distribution in a GaAs quantum well in AlGaAs for parameters $T = 300\text{K}$, $m = 0.07m_e$, well width 10 nm and a electron density of $n = 1.2 \cdot 10^{13} m^{-2}$ (a) for a free standing quantum well, (b) in GaAs barrier phonons (c) including finite sample boundaries and (d) additionally with AlAs phonons.

emission. Emission perpendicular to the quantum well is observed, cf. Fig. 4. This geometry selects intraband emission for the electron gas (not intersubband processes), since the dipole moment is in-plane with the quantum well and leads to a mostly perpendicular emission. The quantum light emission is calculated using a correlation expansion approach in second-order Born approximation and describes a momentum and energy conservation ensuring joint process of electron-phonon and electron-photon interaction. We find the following formula for the stationary light emission of a specific mode $\boldsymbol{k}, \sigma$ [32, 13]:

$$\begin{aligned}\partial_t m_{\boldsymbol{k}\sigma} = \sum_{\boldsymbol{cq}} 2\pi |g_{\boldsymbol{q}}|^2 |\zeta(\omega_{\boldsymbol{k}\sigma})|^2 |F^{\boldsymbol{q}}_{\boldsymbol{qk}\sigma}|^2 f_{\boldsymbol{c}+\boldsymbol{q}_\parallel}(1-f_{\boldsymbol{c}}) \cdot \\ \cdot \big[(1+n_{\boldsymbol{q}})\, \delta(\omega_{\boldsymbol{k}\sigma} + \varepsilon_{\boldsymbol{c}} - \varepsilon_{\boldsymbol{c}+\boldsymbol{q}_\parallel} + \omega_{LO}) \\ + n_{\boldsymbol{q}}\, \delta(\omega_{\boldsymbol{k}\sigma} + \varepsilon_{\boldsymbol{c}} - \varepsilon_{\boldsymbol{c}+\boldsymbol{q}_\parallel} - \omega_{LO})\big]\,, \qquad (10)\end{aligned}$$

where ζ is the Heitler-Zeta function and $m_{\boldsymbol{k}\sigma}$ is the photon number, which is directly connected to the observed stationary emission spectra $S(\omega_{\boldsymbol{k}\sigma}) \propto \hbar\omega_{\boldsymbol{k}\sigma}\partial_t m_{\boldsymbol{k}\sigma}$. Inspecting the spectra given by Eq. (10) shows, that the photons are generated through the stimulated/spontaneous emission $(1+n_{\boldsymbol{q}})$ or the induced absorption $(n_{\boldsymbol{q}})$ of a phonons , where $n_{\boldsymbol{q}}$ is the phonon occupation. The emission is propertional to a Pauli blocking term $f_{\boldsymbol{c}+\boldsymbol{q}_\parallel}(1-f_{\boldsymbol{c}})$ and the phonon occupation, jointly participating in the emission process. The argument of the delta function ensures energy conservation. It is possible to evaluate Eq. (10)

with different quantization schemes for the photons, cf. Fig. 5. In Fig. 5 (a) the electron gas of a free standing quantum well in vacuum leads to a broad THz emission spectrum with an enhancement at the TO-phonon-frequency. After including also barrier TO-phonons inside an infinitely extended sample [cf. Fig. 5 (b)], the emission at the TO-phonon frequency is furthermore intensified and a longitudinal-transversal splitting between LO- and TO-phonon frequency appears. Considering additionally the geometric constrains due to a finite sample in the quantization, the emission at the LO-frequency is intensified while it is suppressed at the TO-frequency (cf. Fig. 5 (c)). This occurs because the photon modes in the finite sample geometry at LO-frequency are stronger at the quantum well position while the TO-frequency modes are reduced at this position. Furthermore, in Fig. 5 (d) also AlAs-like phonons of the barrier material are included.

Obviously the quantum light THz emission from intrasubband processes inside a quantum well is assisted by electron-phonon relaxation and is strongly influenced by the TO-phonons of the sample.

7 Summary

We have applied a non-equilibrium density matrix approach to a broad variety of 2D electron gases. Based on a unified approach for the electron-phonon interaction, the combined electron-phonon dynamics is shown to determine the features of electron cooling and their spatiotemporal propagation in systems of different character: silicon surfaces, THz quantum cascade lasers, graphene, and GaAs quantum wells.

Acknowledgement

We acknowledge support from the Deutsche Forschungsgemeinschaft through KN 427, Sfb 787 and CoE UniCAT.

References

1. R. Huber, R. A. Kaindl, B. A. Schmid, D. S. Chemla: Broadband terahertz study of excitonic resonances in the high-density regime in $GaAs/Al_xGa_{1-x}As$ quantum wells, Phys. Rev. B **72**, 161314 (2005)
2. T. Shih, K. Reimann, M. Woerner, T. Elsaesser, I. Waldmüller, A. Knorr, R. Hey, K. H. Ploog: Nonlinear response of radiatively coupled intersubband transitions of quasi-two-dimensional electrons, Phys. Rev. B. **72**, 195338 (2005)
3. Z. Wang, K. Reimann, M. Woerner, T. Elsaesser, D. Hofstetter, J. Hwang, W. J. Schaff, L. F. Eastman: Optical phonon sidebands of electronic intersubband absorption in strongly polar semiconductor heterostructures, Phys. Rev. Lett. **94**, 037403 (2005)

4. P. R. Wallace: The band theory of graphite, Phys. Rev. **71**, 622–634 (1947)
5. K. S. Novoselov, A. K. Geim, S. V. Morozov, D. Jiang, Y. Zhang, S. V. Dubonos, I. V. Grigorieva, A. A. Firsov: Electric field effect in atomically thin carbon films, Science **306**, 666–669 (2004)
6. T. Kampfrath, L. Perfetti, F. Schapper, C. Frischkorn, M. Wolf: Strongly coupled optical phonons in the ultrafast dynamics of the electronic energy and current relaxation in graphite, Phys. Rev. Lett. **95**, 187403 (2005)
7. S. Tanaka, K. Tanimura: Time-resolved two-photon photoelectron spectroscopy of the Si(001)-(2×1) surface, Surf. Science **529**, 251 (2003)
8. M. Weinelt, M. Kutschera, T. Fauster, M. Rohlfing: Dynamics of exciton formation at the Si(100) $c(4 \times 2)$ surface, Phys. Rev. Lett. **92**, 126801 (2004)
9. A. Thränhardt, S. Kuckenburg, A. Knorr, T. Meier, S. W. Koch: Quantum theory of phonon-assisted exciton formation and luminescence in semiconductor quantum wells, Phys. Rev. B **62**, 2706–2720 (2000)
10. F. Rossi, T. Kuhn: Theory of ultrafast phenomena in photoexcited semiconductors, Rev. Mod. Phys. **74**, 895–950 (2002)
11. N. Buecking, P. Kratzer, M. Scheffler, A. Knorr: Theory of optical excitation and relaxation phenomena at semiconductor surfaces: linking density functional and density matrix theory, Appl. Phys. A **88**, 505 (2007)
12. M. Kira, W. Hoyer, S. W. Koch: Microscopic theory of the semiconductor terahertz response, Phys. Status Solidi B **238**, 443–450 (2003)
13. M. Richter, S. Butscher, M. Schaarschmidt, A. Knorr: Model of thermal terahertz light emission of a two-dimensional electron gas, Phys. Rev. B **75**, 115331 (2007)
14. S. Butscher, A. Knorr: Theory of strong electron-phonon coupling for ultrafast intersubband excitations, Phys. Status Solidi B **243**, 2423–2427 (2006)
15. N. Buecking, S.Butscher, M. Richter, C.Weber, S. Declair, M. Woerner, Kreimann, P. Kratzer, M. Scheffler, A. Knorr: Theory of electron-phonon interactions on nanoscales: semiconductor surfaces and two dimesional electron gases, in *Proceedings of SPIE 6892* (2008)
16. S. Butscher, F. Milde, M. Hirtschulz, E. Malic, A. Knorr: Hot electron relaxation and phonon dynamics in graphene, Appl. Phys. Lett. **91**, 203103 (2007)
17. A. Thrnhardt, I. Kuznetsova, C. Schlichenmaier, S. W. Koch, L. Shterengas, G. Belenky, J.-Y. Yeh, L. J. Mawst, N. Tansu, J. Hader, J. V. Moloney, W. W. Chow: Nitrogen incorporation effects on gain properties of gainnas lasers: Experiment and theory, Applied Physics Letters **86**, 201117 (2005)
18. J. Dabrowski, M. Scheffler: Self-consistent study of the electronic and structural properties of the clean Si(001)(2x1) surface, Appl. Surf. Sci. **56**, 15 (1992)
19. N. Buecking, P. Kratzer, M. Scheffler, A. Knorr: Linking density-functional and density-matrix theory: picosecond electron relaxation at the Si(100) surface, Phys. Rev. B (2008) (accepted)
20. C. Gmachl, F. Capasso, D. L. Sivco, A. Y. Cho: Recent progress in quantum cascade lasers and applications, Rep. Prog. Phys. **64**, 1533–1601 (2001)
21. B. S. Williams: Terahertz quantum-cascade lasers, Nature Photonics **1**, 517 (2007)
22. C. Weber, F. Banit, S. Butscher, A. Knorr, A. Wacker: Theory of the ultrafast nonlinear response of terahertz quantum cascade laser structures, Appl. Phys. Lett. **89**, 091112 (2006)

23. S. Kumar, B. S. Williams, S. Kohen, Q. Hu, J. L. Reno: Continuous-wave operation of terahertz quantum-cascade lasers above liquid-nitrogen temperature, Appl. Phys. Lett. **84**, 2494–2496 (2004)
24. F. Eickemeyer, K. Reimann, M. Woerner, T. Elsaesser, S. Barbieri, C. Sirtori, G. Strasser, T. Müller, R. Bratschitsch, K. Unterrainer: Ultrafast Coherent Electron Transport in Semiconductor Quantum Cascade Structures, Phys. Rev. Lett. **89**, 047402 (2002)
25. M. Woerner, K. Reimann, T. Elsaesser: Coherent charge transport in semiconductor quantum cascade structures, J. Phys.: Condens. Matter **16**, R25–R48 (2004)
26. A. Bostwick, T. Ohta, T. Seyller, K. Horn, E. Rotenberg: Quasiparticle dynamics in graphene, Nat. Phys. **3**, 36–40 (2007)
27. S. Piscanec, M. Lazzeri, F. M. A. C. Ferrari, J. Robertson: Kohn anomalies and electron-phonon interactions in graphite, Phys. Rev. Lett. **93**, 185503 (2004)
28. A. Grueneis, R. Saito, G. G. Samsonidze, T. Kimura, M. A. Pimenta, A. Jorio, A. G. S. Fihho, G. Dresselhaus, M. S. Dresselhaus: Inhomogeneous optical absorption around the k point in graphite and carbon nanotubes, Phys. Rev. B **67**, 165402 (2003)
29. D. J. Santos, R. Loudon: Electromagnetic-field quantization in inhomogeneous and dispersive one-dimensional systems, Phys. Rev. A **52**, 1538 (1995)
30. Z. Lenac: Quantum optics of dispersive dielectric media, Phys. Rev. A **68**, 063815 (2003)
31. W. Hoyer, M. Kira, S. W. Koch, J. V. Moloney, E. M. Wright: Light-matter interaction in finite-size plasma systems, Phys. Status Solidi (b) **244**, 3540–3557 (2007)
32. M. Richter, M. Schaarschmidt, A. Knorr, W. Hoyer, J. V. Moloney, E. M. Wright, M. Kira, S. W. Koch: Quantum theory of incoherent THz emission of an interacting electron-ion plasma, Phys. Rev. A **71**, 053819 (2005)